Neoplasia • Vol. 7, No. 10, October 2005, pp. 904–911

www.neoplasia.com

Nanoparticles for the Optical Imaging of Tumor E-selectin[1]

Martin Funovics[*,2], *Xavier Montet*[†,2], *Fred Reynolds*[†], *Ralph Weissleder*[†] *and Lee Josephson*[†]

*Department of Angiography and Interventional Radiology, Vienna Medical University, Vienna, Austria; [†]Center for Molecular Imaging Research, Massachusetts General Hospital and Harvard Medical School, Charlestown, MA, USA

Abstract

We designed a fluorescent peptide–magnetic nanoparticle conjugate that images E-selectin expression in mouse xenograft models of Lewis lung carcinoma (LLC) by fluorescence reflectance imaging. It was synthesized by attaching the E-selectin–binding peptide (ESBP; CDSDSDITWDQLWDLMK) to a CLIO(Cy5.5) nanoparticle to yield ESBP–CLIO(Cy5.5). Internalization by activated human umbilical vein endothelial cells (HUVECs) was rapid and mediated by E-selectin, indicated by the lack of uptake of nanoparticles bearing similar numbers of a scrambled peptide (Scram). To demonstrate the specificity of E-selectin targeting to ESBP–CLIO(Cy5.5) *in vivo*, we coinjected ESBP–CLIO (Cy5.5) and Scram–CLIO(Cy3.5) and demonstrated a high Cy5.5/Cy3.5 fluorescence ratio using the LLC. Histology showed that ESBP–CLIO was associated with tumor cells as well as endothelial cells, but fluorescence-activated cell sorter analysis showed a far less expression of E-selectin on LLC than on HUVECs. Using immunohistochemistry, we demonstrated E-selectin expression in both endothelial cells and cancer cells in human prostate cancer specimens. We conclude that ESBP–CLIO (Cy5.5) is a useful probe for imaging E-selectin associated with the LLC tumor, and that E-selectin is expressed not only on endothelial cells but also on LLC cells and human prostate cancer specimens.

Neoplasia (2005) **7,** 904–911

Keywords: Nanoparticle, E-selectin, Lewis lung carcinoma, peptide, internalization.

Introduction

Selectins (E-, P-, and L-selectin) are a family of cell surface glycoproteins that mediate interactions between leukocytes and endothelial cells [1]. E-selectin is a C-type lectin of 97 kDa that binds to the tetrasaccharide sialyl Lewis X structure, which appears to be a minimal ligand involved in cell adhesion [2–4]. E-selectin (CD62E and endothelial leukocyte adhesion molecule 1) is upregulated in endothelia by cytokines such as interleukin 1β (IL-1β) or tumor necrosis factor α, and is an early marker for the detection of inflammation [5,6]. Although less established in inflammation and leukocyte migration, there is considerable evidence that an interaction between E-selectin and cancer cells may be involved in adhesion and metastases [7–9].

To develop a nanoparticle binding E-selectin, we conjugated peptides containing the DITWDQLWDLMK E-selectin–binding sequence to amino–CLIO(Cy5.5), a crosslinked dextran-coated iron oxide nanoparticle that is widely used for the attachment of biomolecules for *in vitro* and *in vivo* applications [10–12]. Peptides containing this sequence, termed E-selectin–binding peptides (ESBPs), bind E-selectin (but not P-selectin or L-selectin) noncompetitively with sialyl Lewis X with a dissociation constant of 3 to 5 nM and have a similar affinity for mouse or human E-selectins [13,14]. Mouse and human E-selectins have a 73% sequence homology and many common immunologic determinants [15]. Probes using this sequence lack species specificity and can be used to target E-selectin in a wide variety of animal models and, potentially, clinically. In contrast, nanoparticles using a monoclonal antibody bind human E-selectin, but not mouse E-selectin [16,17], which prevents them from being used in animal models like the Lewis lung carcinoma (LLC) model used here.

We used the fluorescence of the ESBP–CLIO(Cy5.5) nanoparticle to monitor its interaction with LLC cells *in vitro* and by fluorescence reflectance imaging *in vivo*. With the LLC, fluorescence microscopy indicated that ESBP–CLIO(Cy5.5) was not associated with endothelial cells, as might be expected based on the function of E-selectin, but was present in both tumor and endothelial cells. We next examined histochemically the expression of E-selectin on human prostate cancer specimens and demonstrated that it was a frequently expressed marker. We conclude that the ESBP–CLIO(Cy5.5) nanoparticle can be used for imaging E-selectin expression by fluorescence reflectance and that E-selectin is expressed on both tumor and endothelial cells.

Address all correspondence to: Lee Josephson, PhD, Center for Molecular Imaging Research, Massachusetts General Hospital, Building 149, 13th Street, No. 5406, Charlestown, MA 02129. E-mail: ljosephson@partners.org

[1]This work was supported by R01-EB00662. X.M. was supported by a fellowship from the Swiss National Science Foundation.

[2]Martin Funovics and Xavier Montet contributed equally to this work.

Received 10 May 2005; Revised 20 June 2005; Accepted 23 June 2005.

DOI 10.1593/neo.05352

Methods

Peptides were synthesized by an Apex 396 peptide synthesizer using a standard solid-phase Fmoc chemistry (Advanced Chemtech, Lousiville, KY) and were purified by reverse-phase high-performance liquid chromatography, as described [12,18]. The peptides used were (FITC)BCDSDSDITWDQLWDLMKNH2 (ESBP) and (FITC)BCDSDSKMIDWTWLQLDD-NH2 (scrambled peptide or Scram). "B" stands for β-alanine. The identity and purity of peptides were confirmed by mass spectroscopy. The amino–CLIO nanoparticle (crosslinked iron oxide) was synthesized as described and iron-assayed spectrophotometrically [11,12].

The linker chemistry for the E-selectin conjugating peptides to magneto-optical nanoparticles has been described in detail (see Figure 1 of Ref. [18]). A fluorochrome (Cy3.5 or Cy5.5; Amersham Biosciences Corp., Piscataway, NJ) was first attached directly to the crosslinked dextran coating of the amino–CLIO nanoparticle, consuming one to two of the available 40 to 60 amino groups per nanoparticle and leaving many groups for further modification (e.g., attaching a subsequent peptide to the nanoparticle) [18,19].

To synthesize E-selectin–binding peptide–nanoparticle conjugates, amino–CLIO nanoparticles [10 mg/ml Fe, 2 mg, in phosphate-buffered saline (PBS)] were placed in a tube, and approximately 500 μg of Cy3.5 or Cy5.5 was added. After 2 hours at room temperature, succinimidyl iodoacetic acid (SIA; 140 mM in 100 μl of DMSO) was added, and the mixture was allowed to stand for 1 hour. Unreacted dye and SIA were removed using P-10 spin columns equilibrated in 0.02 M citrate and 0.15 M NaCl (pH 8). The peptides in DMSO were added at a concentration of 0.5 mg peptide/mg Fe to yield nanoparticles with approximately 30 peptides per nanoparticle. The average amount of attached peptides was determined using the absorbance of fluorescein [12]. The average number of peptides per nanoparticle was calculated by assuming 8000 Fe/CLIO nanoparticle [20].

Human umbilical vein endothelial cells (HUVECs; Clonetics, Baltimore, MD) were cultured in an endothelial growth medium (Clonetics). Cells were stimulated to upregulate E-selectin by an exposure to recombinant human IL-1β (Fisher Scientific, Fairlawn, NJ) at a final concentration of 2 ng/ml for 4 hours. LLC cells (ATCC, Manassas, VA) were cultured in Dulbecco's modified Eagle's medium, with 4 mM L-glutamine adjusted to contain 1.5 g/l sodium bicarbonate, 4.5 g/l glucose, 100 U/ml penicillin, 100 μg/ml streptomycin, and 10% fetal bovine serum (all culture supplements were from Invitrogen Corp., Paisley, Scotland, UK).

Nanoparticles were incubated with HUVECs (stimulated or unstimulated) as above (8 μg/ml Fe, 8 hours). Cells were washed three times in PBS, detached with 0.1% Trypsin–EDTA (2 minutes at 37°C), suspended in a cell culture medium at 4°C, and centrifuged (900*g* for 5 minutes). Cells were resuspended in a cell culture medium and kept on ice, and flow cytometry was performed (FacsCalibur; Becton Dickinson, Franklin Lakes, NJ). Relative median fluorescence intensity (Cy5.5 channel) was obtained as a measure of nanoparticle accumulation.

To obtain the concentration and time dependence of the uptake of ESBP–CLIO(Cy5.5) by HUVECs (Figure 1, *C* and *D*), confluent layers of IL-1β–stimulated cells in 24-well plates were incubated with ESBP–CLIO(Cy5.5) in a complete cell culture medium for 8 hours at 37°C. The uptake was measured using an FITC hapten immunoassay for immunoreactive FITC attached to the nanoparticle. Briefly, cells were washed three times with PBS and lysed with PBS containing 0.1% bovine serum albumin (BSA), 0.1% Triton X-100, and 1 mM

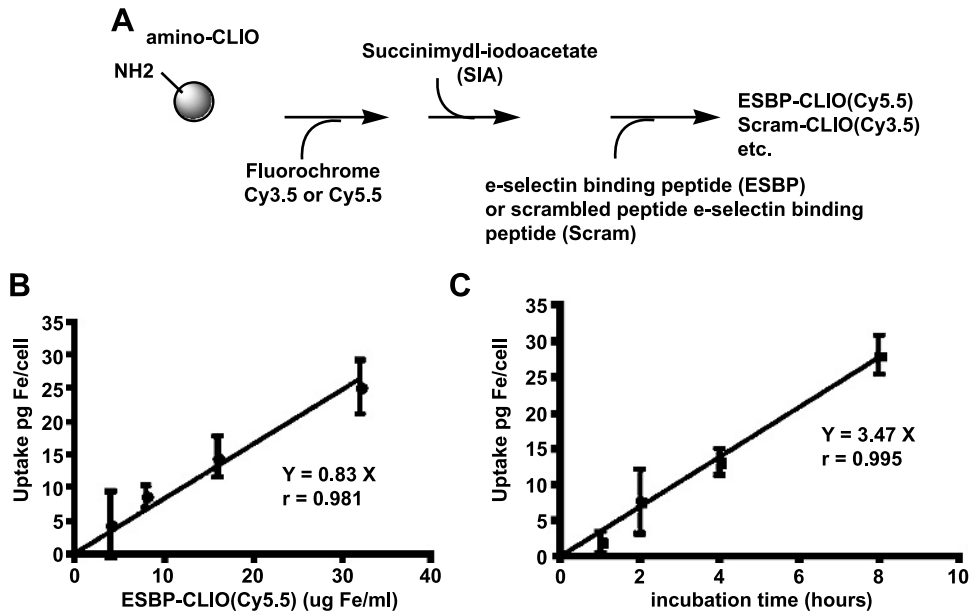

Figure 1. *Synthesis and activity of ESBP–nanoparticle conjugates. (A) Peptides containing the ESBP sequence DITWDQLWDLMK or a scrambled sequence were conjugated to either Cy5.5- or Cy3.5-labeled nanoparticles. (B) The uptake of ESBP–CLIO(Cy5.5) as a function of concentration. (C) The uptake of ESBP–CLIO(Cy5.5) as a function of time. IL-1β–stimulated HUVECs were used for (B) and (C). The nanoparticle concentration was 8 μg/ml Fe in (C).*

8-anilino-1-naphthalenesulfonic acid (1 ml/well). The lysate was first reacted overnight at 4°C with an anti-FITC horseradish peroxidase conjugate (Molecular Probes, Eugene, OR) at 40 ng/ml, and the mixture was then transferred onto a 96-well plate (200 μl/well, MaxiSorp Nunc, eBioscience, San Diego, CA) coated with 12.5 ng/ml FITC-labeled BSA (Sigma-Aldrich, St. Louis, MO). The plates were then washed three times (PBS, 0.1% BSA, and 0.1% Triton X-100), and horseradish peroxidase activity was quantitated at 650 nm using 200 μl of 3,3′,5,5′ tetramethylbenzidine dihydrochloride after a 30-minute incubation at room temperature. Lysate iron concentrations were calculated from a displacement immunoassay standard curve using nanoparticle standards in a lysis medium. The number of cells per well was determined by trypsinizing and counting cells in a hemocytometer. A more complete description of the assay has been provided [21].

To study the specificity of ESBP–CLIO(Cy5.5) interactions to E-selectin (Figure 2), HUVECs were grown on fibronectin-coated coverslips. At 8 μg/ml Fe, ESBP–CLIO(Cy5.5) or Scram–CLIO(Cy3.5) was added to IL-1β–stimulated and unstimulated confluent cell layers for 4 hours. During the last hour, a phycoerythrin (PE)–labeled mouse antihuman E-selectin antibody (BD Pharmingen, San Jose, CA) at 5 μg/ml was added. Cells were then washed three times with PBS, fixed in 2% paraformaldehyde, and mounted. Fluorescence images were obtained using a confocal microscope (Axiovert 200, Plan-Neofluar 40×; Zeiss, Jena, Germany) with laser excitations at 488 nm (FITC) and 543 nm (PE). Image acquisition and analysis were done using the LSM 5 PASCAL Software (Zeiss). For dual-wavelength flow cytometry, cells were detached and suspended as described above.

For dual-fluorochrome *in vivo* imaging (Figure 3), animals were treated in compliance with institutional and legal requirements. Eight nude mice (nu/nu; Charles River Laboratories, Boston, MA) underwent an injection of 2 million LLC cells into the left and right paralumbar regions. After 10 to 14 days, tumors were between 8 and 14 mm in diameter. Animals were anesthetized with 1.5% isofluorane in oxygen and imaged preinjection and 2, 4, 8, and 24 hours postinjection of an intravenous solution with a mixture of approximately 2 to 4 mg Fe/kg ESBP–CLIO(Cy5.5) and 2 to 4 mg Fe/kg Scram–CLIO(Cy3.5), with a final adjustment in concentration to provide for injections of equal fluorescence from each probe. White light and Cy5.5 and Cy3.5 fluorescent images were obtained with a custom-built whole-body mouse optical imaging system described previously [22,23], which was capable of multichannel fluorescent imaging without a significant spectral overlap. Digital images (16 bit) were acquired. Fluorescence intensity was quantitated as a region of interest of constant size comprising 96 pixels at the center of the maximum intensity of the tumor and on adjacent nontumoral tissues. Tumor fluorescence was computed as the tumor-to-background ratio, which was the ratio of the average signal intensity of the tumor divided by the average signal intensity of normal tissues adjacent to the tumor, the boundaries of which were easily visible (Figure 3*A*). After the last time point, the animals were sacrificed with an injection of pentobarbital sodium (100 mg/kg, i.p.), and tissues were processed for histology.

For histology (Figure 4), tumors were excised, placed in a freezing medium (Fisher Scientific), and frozen on dry ice. Cryosections (8 μm in thickness) were obtained, air-dried, fixed with acetone, blocked with PBS containing 0.5% donkey serum and 2% BSA, and incubated with a rat anti-mouse E-selectin (BD Pharmingen) at 1:100 or a rat anti-mouse CD31 at 1:200 (Molecular Probes). A secondary antibody (donkey anti-rat Cy3; Molecular Probes) was applied at 1:500 for 1.5 hours. Nuclei were stained with Sytox green (Molecular Probes) diluted 1:100,000 in PBS for 5 minutes. Sections were imaged using a confocal fluorescence microscope (Axiovert 200; Zeiss). Liver, spleen, and kidney sections served as E-selectin–negative controls, and mouse ear sections from a diazolone-induced hypersensitivity reaction (courtesy of Dr. Rainer Kunstfeld, Cutaneous Biology Research Center, Charlestown, MA) served as positive controls (data not shown).

To examine the expression of E-selectin by LLC cells in culture (Figure 5), cells were grown in Dulbecco's modified Eagle's medium with 4 mM L-glutamine, 1.5 g/l sodium bicarbonate, 4.5 g/l glucose, and 10% fetal bovine serum. Confluent LLC layers were incubated with ESBP–CLIO(Cy5.5) or Scram–CLIO(Cy3.5) (8 μg/ml Fe, 8 hours) and 2 μg/ml rat anti-mouse E-selectin (BD Pharmingen) for 1 hour at 37°C. Cell detachment and flow cytometry were performed as described in Figure 3.

To determine the expression of E-selectin in human prostate cancers (Figure 6), 72 samples from histologically confirmed prostate adenocarcinomas were obtained (Dr. M. Rubin, Department of Pathology, Harvard Medical School, Charlestown, MA). Indigenous avidin and biotin were blocked using the Vector avidin–biotin blocking kit (Vector Laboratories, Burlingame, CA), followed by incubation of the samples with either E-selectin–specific monoclonal antibody IgG ab8165 (Abcam, Inc., Cambridge, MA) or GFP-specific monoclonal antibody IgG (Alpha Diagnostic International, San Antonio, TX) as a negative control at 1 μg/ml. The antibody was detected by a biotinylated secondary goat anti-mouse IgG ab6788 (Abcam, Inc.), diluted 1:200 in PBS, and developed for 8 minutes using the Vectastain Elite ABC kit (Vector Laboratories). Counterstaining was performed in hematoxylin for 1 minute. The samples were rated as highly positive when >75% of the cells were positive, medium positive when 50% to 75% of the cells were positive, low positive when 25% to 50% of the cells were positive, and negative when less than 25% of the cells were positive.

Results

Peptide–nanoparticle conjugates were synthesized with either E-selectin binding (ESBP) or Scram and either Cy5.5 or Cy3.5 (as shown in Figure 1*A*), and were tested for interactions with IL-β–stimulated and unstimulated HUVECs.

We next examined the concentration and time dependence of the uptake of ESBP–CLIO(Cy5.5) with IL-1β–stimulated HUVECs. The uptake of ESBP–CLIO(Cy5.5)

was proportional to nanoparticle concentration (1–30 μg/ml Fe) and time (0–8 hours), as shown in Figure 1, *B* and *C*. The rate of uptake of ESBP–CLIO(Cy5.5) was 3.47 pg/cell Fe per hour at 8 μg/ml Fe. Consistent with the observations of Martens et al. [14], an N-terminal attachment was found to be essential for preserving the E-selectin–binding activity of DITWDQLWDLMK-based peptide–nanoparticle conjugates (data not shown).

The specificity of the interaction of ESBP–CLIO(Cy5.5) to E-selectin *in vitro* was further examined as shown in Figure 2. Figure 2*A* shows confocal fluorescent micrographs of HUVECs incubated with ESBP–CLIO(Cy5.5) with or without IL-1β. IL-1β treatment increased the accumulation of ESBP–CLIO(Cy5.5) nanoparticles that are visible throughout the cytoplasm as punctate centers of fluorescence. The uptake of the control nanoparticle, Scram–CLIO(Cy3.5),

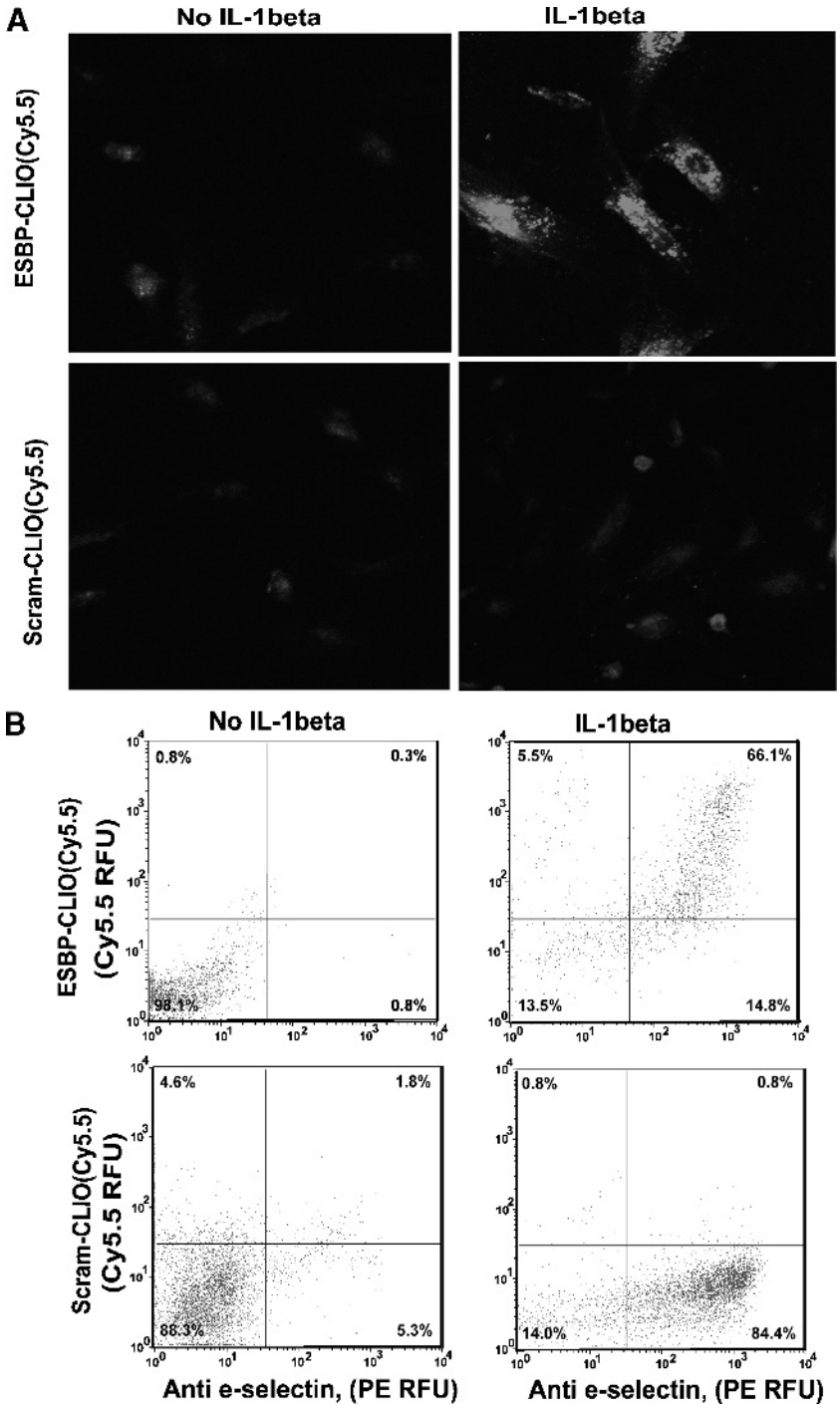

Figure 2. *Specificity of ESBP–CLIO(Cy5.5) interaction to E-selectin. (A) Confocal microscopy of ESBP–CLIO(Cy5.5) and Scram–CLIO(Cy3.5) uptake by HUVECs with and without IL-1β. (B) Dual-wavelength fluorescence-activated cell sorter (FACS) uptake of ESBP–CLIO(Cy5.5) and Scram–CLIO(Cy5.5) by HUVECs with and without IL-1β.*

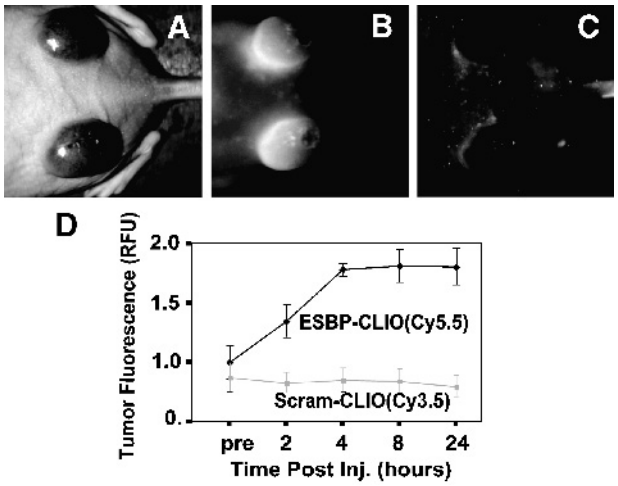

Figure 3. *Imaging of E-selectin with ESBP–CLIO(Cy5.5) in the LLC. LLCs were implanted in nude mice followed by injection with a mixture of ESBP–CLIO(Cy5.5) and the control nanoparticle, Scram–CLIO(Cy3.5), at 3 mg/kg Fe each. White light image (A), Cy5.5 fluorescence (B), and Cy3.5 fluorescence (C) are shown 24 hours after injection. The Cy5.5 channel shows a high fluorescence, whereas the Cy3.5 channel shows none. (D) The time course of the fluorescence of tumor-to-background ratios in the Cy5.5 and Cy3.5 channels.*

was lower and was not stimulated by IL-1β. To further examine the specificity of the interaction of ESBP–CLIO(Cy5.5) to E-selectin, HUVECs were examined by the dual-wavelength flow cytometry (Figure 2*B*). Here the uptake of ESBP–CLIO(Cy5.5)–labeled Cy5.5 nanoparticles was compared with the binding of a PE-labeled anti-human E-selectin. As expected, IL-1β treatment increased E-selectin expression, and cells expressing E-selectin internalized ESBP–CLIO(Cy5.5). However, IL-1β treatment failed to increase the uptake of Scram–CLIO(Cy5.5).

We next examined the specificity of the interaction of ESBP–CLIO(Cy5.5) to E-selectin *in vivo*, as shown in Figure 3. A mouse xenograft model of LLC was used as a model of E-selectin–expressing tissue because it is a rapidly growing tumor and is an excellent source of small blood vessels, which express E-selectin [24]. We examined nanoparticle accumulation in LLC using dual-channel intravital fluorescence microscopy, as shown in Figure 4. Figure 3 shows white light (*A*), Cy5.5 fluorescence (*B*), and Cy3.5 fluorescence (*C*) images for the LLC xenograft model at various time points after the coinjection of both probes. The accumulation of Cy3.5 fluorescence by LLC was similar to the background, whereas Cy5.5 fluorescence was markedly increased. The time course of the tumor fluorescence ratio is shown in Figure 3*D*. Cy5.5 fluorescence increased, slowly reaching a plateau at about 4 hours postinjection, whereas Cy3.5 fluorescence was unchanged or decreased slightly. Because Cy5.5 and Cy3.5 were both attached to nanoparticle probes that matched in size, linker chemistry, and composition of attached amino acids and differed only in peptide sequence, the increase in Cy5.5 fluorescence indicated that ESBP–CLIO(Cy5.5) specifically bound E-selectin *in vivo*. Our data suggest a plasma half-life of roughly 1 to 2 hours for ESBP–CLIO(Cy5.5) because the plateau of

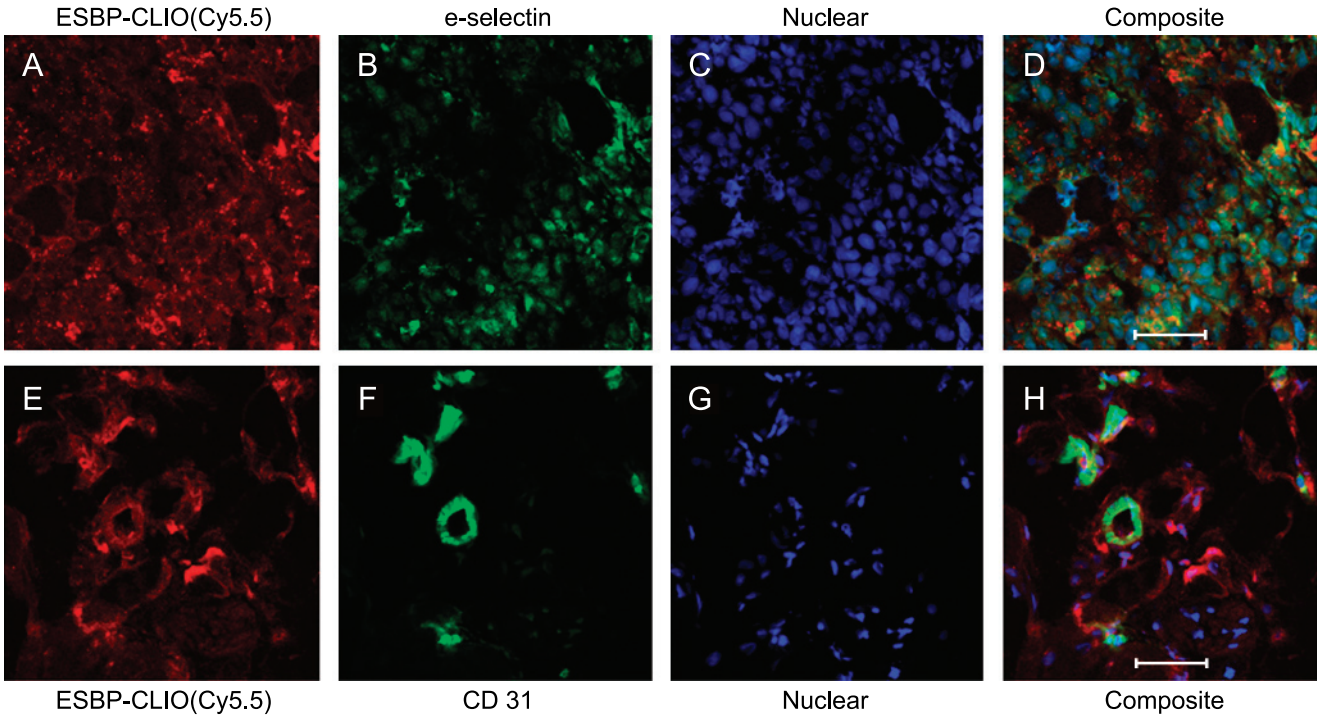

Figure 4. *Confocal microscopy to determine the cellular distribution of ESBPCLIO(Cy5.5) in LLC. The top row (A–D) is a single section. (A) ESBP–CLIO(Cy5.5) is shown as the distribution of Cy5.5 fluorescence at 24 hours postinjection. (B) E-selectin visualized with anti–E-selectin (Cy3.5 second antibody fluorescence). (C) Nuclear stain. (D) Composite of (A)–(C). The bottom row is a second single section. (E) ESBP–CLIO(Cy5.5) fluorescence. (F) CD31 visualized with anti-CD31. (G) Nuclear stain. (H) Composite of (E)–(G). Scale bar, 20 μm.*

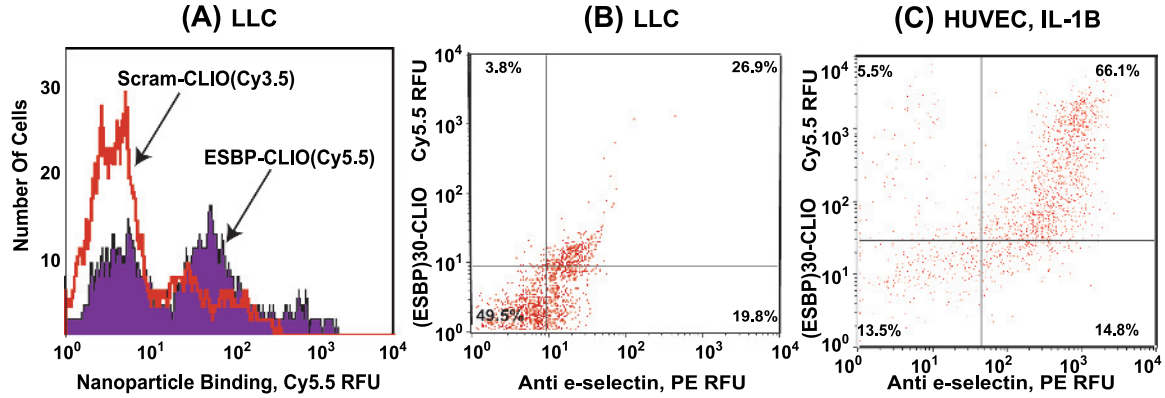

Figure 5. *Binding of ESBP–CLIO(Cy5.5) to LLC. (A) LLC cells were incubated with ESBP–CLIO(Cy5.5) or Scram–CLIO(Cy3.5), and binding by single-channel FACS was determined. (B) The binding of ESBP–CLIO(Cy5.5) to LLC is analyzed by dual-wavelength FACS. (C) The binding of ESBP–CLIO(Cy5.5) to IL-1β–stimulated HUVECs from Figure 2B is shown for comparison.*

tumor fluorescence was reached by 4 hours postinjection and accumulation was not maximal at the initial 2-hour time point. In mice, plasma half-lives range from 47 minutes for a tat–CLIO conjugate to 650 minutes for the nonpeptide-conjugated parent CLIO nanoparticle [25]. It appears that the uptake of ESBP–CLIO(Cy5.5) is mediated by E-selectin *in vitro* and *in vivo*.

LLC tumors were then submitted for histology to determine the cells accumulating ESBP–CLIO(Cy5.5), as shown in Figure 4. Two representative sections of the tumors are shown with a different series of stains: one set where E-selectin is visualized (Figure 4, *A–D*) and a second set where CD31, an endothelial cell marker, is visualized (Figure 4, *E–H*). ESBP–CLIO(Cy5.5) is visualized as Cy5.5 fluorescence, as shown in Figure 4, *A* and *E*. To demonstrate the expected association of ESBP–CLIO(Cy5.5) uptake with E-selectin expression on endothelial cells, we stained sections with anti-CD31 (Figure 4*F*). However, we found that ESBP–CLIO(Cy5.5) was associated with both strongly CD31-positive cells and non–CD31-staining cells. A composite of Figure 4, *A* and *B* is shown in Figure 4*D*, together with an additional nuclear stain (Figure 4*C*). It thus appeared that ESBP–CLIO(Cy5.5) was not only associated with endothelial cells but was present on tumor cells as well. To further verify this point, a second tumor section was obtained and stained with anti–E-selectin (Figure 4*B*). Both ESBP–CLIO(Cy5.5) and E-selectin were widely distributed throughout the tumor and were not associated with any specific cells. A composite of Figure 4, *E* and *F* is shown in Figure 4*H*, together with an additional nuclear stain (Figure 4*G*). Although *in vitro* experiments with HUVECs

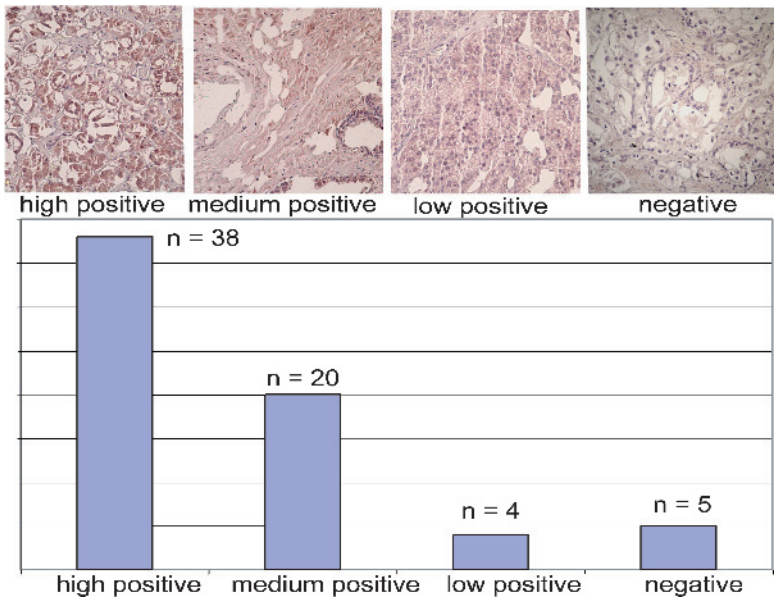

Figure 6. *E-selectin expression in the human prostate. Representative images of specimens rated as high positive, medium positive, low positive, or negative for E-selectin expression by immunohistochemistry are shown. Also shown are the numbers of specimens in each category. Samples were from prostates with histologically confirmed adenocarcinomas.*

indicated that ESBP–CLIO(Cy5.5) was internalized in IL-1β–activated cells by an interaction with E-selectin, it appeared that E-selectin expression and accumulation of ESBP–CLIO (Cy5.5) occurred throughout the tumor.

We next examined whether E-selectin might be expressed on LLC cells grown *in vitro*. Figure 5*A* shows the uptake of ESBP–CLIO(Cy5.5) and Scram–CLIO(Cy3.5) by LLC using a single-channel flow cytometry analysis. With ESBP–CLIO(Cy5.5), both high- and low-binding populations of cells were clearly discernable, whereas with the Scram–CLIO(Cy3.5) nanoparticle, only a single low-binding population was obtained. The accumulation of ESBP–CLIO(Cy5.5) was further examined by the dual-wavelength flow cytometry using PE-labeled anti–E-selectin, as shown in Figure 5*B*. As was the case with the single-channel flow cytometry (Figure 5*A*), a population of cells labeled with both ESBP–CLIO(Cy5.5) and anti–E-selectin was present (26.9% of cells). However, this population appeared to have less ESBP–CLIO(Cy5.5) uptake or E-selectin expression than HUVECs (compare Figure 5, *B* and *C*). Thus, it appears that E-selectin is expressed by LLCs both *in vivo* and *in vitro*, but this expression is at a lower level than that seen when IL-1β induces E-selectin expression on HUVECs. The treatment of LCC with IL-1β had no effect on the binding of ESBP–CLIO(Cy5.5) to LLC (data not shown).

The expression of E-selectin on endothelial cells was well established, but we were unaware of reports of its expression on tumor cells until the recent report [26]. We therefore obtained an array of 72 human prostate specimens from prostates with histologically confirmed adenocarcinomas. Of these, 67 could be evaluated for E-selectin expression by immunohistochemistry. Samples were rated as high positive, medium positive, low positive, and negative, representative specimens of which are shown in Figure 6*A*. As shown in Figure 6*B*, 38 of 67 samples evaluated were rated as strongly positive for E-selectin expression.

Discussion

Specificity

A key issue for molecularly targeted optical nanoparticles is the specificity of their molecular targeting *in vivo*. Determining molecular specificity *in vivo* with peptide–nanoparticle conjugates (10–200 nm) using a peptide to block interactions between a peptide–nanoparticle conjugate and its target is difficult because of limitations of peptide solubility; in addition, the plasma half-life of peptides is often far shorter than the half-life of nanoparticles whose binding they are proposed to inhibit. The problem of demonstrating nanoparticle specificity *in vivo* is exacerbated by the ability of nonmolecularly targeted magnetic nanoparticles to accumulate in diverse types of pathology. Although magnetic nanoparticles accumulate in the normal liver, spleen, and lymph nodes [27–31], their accumulation in a variety of pathologies also occurs. Nontargeted nanoparticle accumulation occurs at the sites of infection [32, 33], in atherosclerotic vessels [34–36], and in rheumatoid arthritis [37]. Nanoparticle accumulation has also been seen in several types of tumors, such as those of the brain [38,39] and head and neck [40]. To minimize the possibility of non–E-selectin–mediated uptake contributing to tissue fluorescence, we used 3 mg Fe/kg ESBP–CLIO(Cy5.5), which was only slightly higher than the clinical dose of 2.6 mg/kg Fe [31]. To determine the molecular specificity of ESBP–CLIO(Cy5.5) *in vivo*, the nanoparticle and Scram–CLIO(Cy3.5) were coinjected and fluorescence reflectance images were obtained using dual-channel fluorescent imaging methods [22]. The progressive increase in the Cy5.5/Cy3.5 ratio in the LLC with time provided evidence of the E-selectin–mediated accumulation of ESBP–CLIO(Cy5.5) *in vivo*.

Sensitivity, Uptake, and the Presence of E-selectin on Tumor Cells

It appears that the fluorescence of ESBP–CLIO(Cy5.5) nanoparticles, when used in conjunction with near-infrared fluorescent imaging, has the sensitivity to detect low levels of E-selectin expression in the LLC. The explanation for this high sensitivity lies in the rapid E-selectin–mediated internalization of ESBP–CLIO(Cy5.5), even at low concentrations. In addition, the binding of ESBP–CLIO(Cy5.5) triggers endocytosis and intracellular accumulation (Figure 2*A*), with negligible nanoparticle loss in the 24-hour period of our longest experiments [18,39]. Finally, when E-selectin–binding ligands are internalized, plasma membrane E-selectin is rapidly replaced [41].

Expression on Human Cells

We found that ESBP–CLIO(Cy5.5) binding and E-selectin expression were not limited to endothelial cells in the LLC both *in vivo* (Figure 4) and *in vitro* (Figure 5). Bhaskar et al. [26] have recently reported that E-selectin mRNA and immunoreactive E-selectin were overexpressed in human prostate cancer specimens even though E-selectin expression was not detected in human cancer cell lines of prostatic origin, normal human tissues, or nonprostatic cancers. We have confirmed the expression of E-selectin in the human prostate cancer epithelium using immunohistochemistry (Figure 6). Our results indicate that E-selectin expression in the LLC model, a tumor of murine origin, can be imaged by optical methods and that E-selectin expression can be detected by immunohistochemistry in human prostate cancer specimens. The lack of expression of E-selectin on cultured human cell lines and xenographs [26], however, means that there is currently no model suitable for imaging E-selectin expression with cancers of human origin. The lack of expression of E-selectin on human prostate cancer cell lines and its expression in human prostatic cancers suggest that unknown tissue-based environmental factors cause its upregulation or downregulation [26] and complicate efforts to study E-selectin function *in vitro*. Thus, the comparison of E-selectin expression on LLC and endothelial cells (Figure 5) may be between cells expressing basal levels of E-selectin (LLC) and those where it is highly upregulated (IL-1β/endothelial cells). Further determinations of which tumor cells express E-selectin, its function, and

the regulation of its expression are questions of considerable interest.

Acknowledgements

We thank Rainer Kunstfeld (Cutaneous Biology Research Center) for providing selectin-positive control sections and for sharing his profound knowledge. We also thank Umar Mahmood for help with optical imaging.

References

[1] Bevilacqua M, Butcher E, Furie B, Gallatin M, Gimbrone M, Harlan J, et al. (1991). Selectins: a family of adhesion receptors. *Cell* **67,** 233.

[2] McEver RP (1997). Selectin–carbohydrate interactions during inflammation and metastasis. *Glycoconj J* **14,** 585–591.

[3] Stoolman LM (1989). Adhesion molecules controlling lymphocyte migration. *Cell* **56,** 907–910.

[4] Phillips ML, Nudelman E, Gaeta FC, Perez M, Singhal AK, Hakomori S, et al. (1990). ELAM-1 mediates cell adhesion by recognition of a carbohydrate ligand, sialyl-Lex. *Science* **250,** 1130–1132.

[5] Haskard DO, Keelan ET, Chapman PT, Robinson M, Binns RM, Jamar F, et al. (1998). Quantifying and imaging activated endothelium in inflammation. *Endothel Cell Res Ser* **4,** 135–149.

[6] Bevilacqua MP, Stengelin S, Gimbrone MA Jr, and Seed B (1989). Endothelial leukocyte adhesion molecule 1: an inducible receptor for neutrophils related to complement regulatory proteins and lectins. *Science* **243,** 1160–1165.

[7] Fukuda MN, Ohvama C, Lowitz K, Matsuo O, Pasqualini R, Ruoslahti E, et al. (2000). A peptide mimic of E-selectin ligand inhibits sialyl Lewis X–dependent lung colonization of tumor cells. *Cancer Res* **60,** 450–456.

[8] Zetter BR (1993). Adhesion molecules in tumor metastasis. *Semin Cancer Biol* **4,** 219–229.

[9] Brodt P, Fallavollita L, Bresalier RS, Meterissian S, Norton CR, and Wolitzky BA (1997). Liver endothelial E-selectin mediates carcinoma cell adhesion and promotes liver metastasis. *Int J Cancer* **71,** 612–619.

[10] Perez JM, Josephson L, O'Loughlin T, Hogemann D, and Weissleder R (2002). Magnetic relaxation switches capable of sensing molecular interactions. *Nat Biotechnol* **20,** 816–820.

[11] Josephson L, Perez JM, and Weissleder R (2001). Magnetic nanosensors for the detection of oligonucleotide sequences. *Angew Chem Int Ed Engl* **40,** 3204–3206.

[12] Josephson L, Tung CH, Moore A, and Weissleder R (1999). High-efficiency intracellular magnetic labeling with novel superparamagnetic–Tat peptide conjugates. *Bioconjug Chem* **10,** 186–191.

[13] Zinn KR, Chaudhuri TR, Smyth CA, Wu Q, Liu H-G, Fleck M, Mountz JD, and Mountz JM (1999). Specific targeting of activated endothelium in rat adjuvant arthritis with a 99mTc-radiolabeled E-selectin–binding peptide. *Arthritis Rheum* **42,** 641–649.

[14] Martens CL, Cwirla SE, Lee RYW, Whitehorn E, Chen EYF, Bakker A, Martin EL, Wagstrom C, Gopalan P, and Smith CW (1995). Peptides which bind to E-selectin and block neutrophil adhesion. *J Biol Chem* **270,** 21129–21136.

[15] Hammel M, Weitz-Schmidt G, Krause A, Moll T, Vestweber D, Zerwes HG, et al. (2001). Species-specific and conserved epitopes on mouse and human E-selectin important for leukocyte adhesion. *Exp Cell Res* **269,** 266–274.

[16] Kang HW, Josephson L, Petrovsky A, Weissleder R, Bogdanov A Jr (2002). Magnetic resonance imaging of inducible E-selectin expression in human endothelial cell culture. *Bioconjug Chem* **13,** 122–127.

[17] Spragg DD, Alford DR, Greferath R, Larsen CE, Lee KD, Gurtner GC, Cybulsky MI, Tosi PF, Nicolau C, and Gimbrone MA Jr (1997). Immunotargeting of liposomes to activated vascular endothelial cells: a strategy for site-selective delivery in the cardiovascular system. *Proc Natl Acad Sci USA* **94,** 8795–8800.

[18] Koch AM, Reynolds F, Kircher MF, Merkle HP, Weissleder R, and Josephson L (2003). Uptake and metabolism of a dual fluorochrome Tat-nanoparticle in HeLa cells. *Bioconjug Chem* **14,** 1115–1121.

[19] Schellenberger EA, Reynolds F, Weissleder R, and Josephson L (2004). Surface-functionalized nanoparticle library yields probes for apoptotic cells. *ChemBioChem* **5,** 275–279.

[20] Reynolds F, O'Loughlin T, Weissleder R, and Josephson L (2005). Method of determining nanoparticle core weight. *Anal Chem* **77,** 814–817.

[21] Kelly KA, Reynolds F, Weissleder R, and Josephson L (2004). FITC-hapten immunoassay for determination of peptide–cell interactions. *Anal Biochem* **330,** 181–185.

[22] Mahmood U, Tung CH, Bogdanov A Jr, and Weissleder R (1999). Near-infrared optical imaging of protease activity for tumor detection. *Radiology* **213,** 866–870.

[23] Mahmood U, Tung CH, Tang Y, and Weissleder R (2002). Feasibility of *in vivo* multichannel optical imaging of gene expression: experimental study in mice. *Radiology* **224,** 446–451.

[24] Allport JR and Weissleder R (2003). Murine Lewis lung carcinoma–derived endothelium expresses markers of endothelial activation and requires tumor-specific extracellular matrix *in vitro*. *Neoplasia* **5,** 205–217.

[25] Wunderbaldinger P, Josephson L, and Weissleder R (2002). Tat peptide directs enhanced clearance and hepatic permeability of magnetic nanoparticles. *Bioconjug Chem* **13,** 264–268.

[26] Bhaskar V, Law DA, Ibsen E, Breinberg D, Cass KM, DuBridge RB, et al. (2003). E-selectin up-regulation allows for targeted drug delivery in prostate cancer. *Cancer Res* **63,** 6387–6394.

[27] Ferrucci JT and Stark DD (1990). Iron oxide–enhanced MR imaging of the liver and spleen: review of the first 5 years. *AJR Am J Roentgenol* **155,** 943–950.

[28] Chen F, Ward J, and Robinson PJ (1999). MR imaging of the liver and spleen: a comparison of the effects on signal intensity of two superparamagnetic iron oxide agents. *Magn Reson Imaging* **17,** 549–556.

[29] Chachuat A and Bonnemain B (1995). European clinical experience with Endorem. A new contrast agent for liver MRI in 1000 patients. *Radiologie* **35,** S274–S276.

[30] Seneterre E, Taourel P, Bouvier Y, Pradel J, Van Beers B, Daures JP, et al. (1996). Detection of hepatic metastases: ferumoxides-enhanced MR imaging *versus* unenhanced MR imaging and CT during arterial portography. *Radiology* **200,** 785–792.

[31] Harisinghani MG, Barentsz J, Hahn PF, Deserno WM, Tabatabaei S, van de Kaa CH, de la Rosette J, and Weissleder R (2003). Noninvasive detection of clinically occult lymph-node metastases in prostate cancer. *N Engl J Med* **348,** 2491–2499.

[32] Gellissen J, Axmann C, Prescher A, Bohndorf K, and Lodemann KP (1999). Extra- and intracellular accumulation of ultrasmall superparamagnetic iron oxides (USPIO) in experimentally induced abscesses of the peripheral soft tissues and their effects on magnetic resonance imaging. *Magn Reson Imaging* **17,** 557–567.

[33] Kaim AH, Wischer T, O'Reilly T, Jundt G, Frohlich J, von Schulthess GK, and Allegrini PR (2002). MR imaging with ultrasmall superparamagnetic iron oxide particles in experimental soft-tissue infections in rats. *Radiology* **225,** 808–814.

[34] Ruehm SG, Corot C, Vogt P, Kolb S, and Debatin JF (2001). Magnetic resonance imaging of atherosclerotic plaque with ultrasmall superparamagnetic particles of iron oxide in hyperlipidemic rabbits. *Circulation* **103,** 415–422.

[35] Schmitz SA, Taupitz M, Wagner S, Wolf KJ, Beyersdorff D, and Hamm B (2001). Magnetic resonance imaging of atherosclerotic plaques using superparamagnetic iron oxide particles. *J Magn Reson Imaging* **14,** 355–361.

[36] Trivedi R, J U-King-Im, and Gillard J (2003). Accumulation of ultrasmall superparamagnetic particles of iron oxide in human atherosclerotic plaque. *Circulation* **108,** e140 (author reply e140).

[37] Dardzinski BJ, Schmithorst VJ, Holland SK, Boivin GP, Imagawa T, Watanabe S, et al. (2001). MR imaging of murine arthritis using ultrasmall superparamagnetic iron oxide particles. *Magn Reson Imaging* **19,** 1209–1216.

[38] Enochs WS, Harsh G, Hochberg F, and Weissleder R (1999). Improved delineation of human brain tumors on MR images using a long- circulating, superparamagnetic iron oxide agent. *J Magn Reson Imaging* **9,** 228–232.

[39] Kircher MF, Allport JR, Graves EE, Love V, Josephson L, Lichtman AH, and Weissleder R (2003). *In vivo* high resolution three-dimensional imaging of antigen-specific cytotoxic T-lymphocyte trafficking to tumors. *Cancer Res* **63,** 6838–6846.

[40] Jonkmanns C, Saleh A, Rees M, and Moedder U (2002). Ultrasmall superparamagnetic iron oxide MIR of head and neck cancer: enhancement of primary tumor and influence on T staging. *Radiology* **225** (supplement), 281.

[41] von Asmuth EJ, Smeets EF, Ginsel LA, Onderwater JJ, Leeuwenberg JF, and Buurman WA (1992). Evidence for endocytosis of E-selectin in human endothelial cells. *Eur J Immunol* **22,** 2519–2526.